Synthesis, Structure, and Magnetic Properties of Ca_3BMnO_6 ($B =$ Ni, Zn) and Ca_3ZnCoO_6 Crystallizing in the K_4CdCl_6 Structure

Shuji Kawasaki and Mikio Takano[1]

Institute for Chemical Research, Kyoto University, Uji, Kyoto-fu 611-0011, Japan

and

Toshiya Inami[2]

Advanced Science Research Center, Japan Atomic Energy Research Institute (JAERI), Tokai-mura, Ibaraki-ken 319-1106, Japan

Ca_3BMnO_6 ($B =$ Ni, Zn) and Ca_3ZnCoO_6 were synthesized and studied by X-ray powder diffraction, neutron powder diffraction, and SQUID magnetometry. All these compounds were found to crystallize in the K_4CdCl_6 structure containing alternate chains made of face-sharing B(II)O_6 trigonal prisms and B'(IV)O_6 octahedra ($B' =$ Mn, Co). Ca_3NiMnO_6 (CNMO) and Ca_3ZnMnO_6 (CZMO) were found to be antiferromagnets with a T_N of 19 and 25.5 K, respectively. CNMO showed a pronounced one-dimensional antiferromagnetic character like a broad susceptibility maximum at 100 K due to short range ordering, while CZMO behaved as a three-dimensional system since the presence of nonmagnetic Zn^{2+} ions suppressed the intrachain exchange interaction. A simple collinear antiferromagnetic structure with an ordered moment of 2.43(15) μ_B/Mn was found in CZMO, while CNMO showed a spiral structure with ordered moments of 2.2(2) μ_B/Mn and 1.4(2) μ_B/Ni. Ca_3ZnCoO_6, on the other hand, showed a ferromagnetic, nonlinear field dependence of magnetization below 90 K, with a hysteresis appearing just below 25 K, and a spontaneous moment measured at 5 K was 0.6 μ_B/Co, suggesting the Co^{4+} ions being in low spin state. © 1999 Academic Press

Key Words: K_4CdCl_6-type oxide; high-pressure synthesis; neutron diffraction; one-dimensional magnetism.

INTRODUCTION

Recently $A_3BB'O_6$ ($A =$ Ca, Sr, ... , $B =$ Ni, Cu, Zn, ... , and $B' =$ Ir, Pt, ...) type oxides of the K_4CdCl_6 structure (1) have been discussed in many reports from a viewpoint of one-dimensional (1D) magnetism. To our knowledge,

the first intensive work was by Nguyen's group (2–4). According to them, Sr_3CuPtO_6 (2), Sr_3CuIrO_6 (3), and $Sr_3CuPt_{0.5}Ir_{0.5}O_6$ (4, 5) are a 1D Heisenberg antiferromagnet, a 1D Heisenberg ferromagnet, and a random quantum spin chain paramagnet, respectively.

These oxides contain alternating chains made of trigonal prisms (BO_6) and octahedra ($B'O_6$) which share their triangular faces with each other. A slip of the typical infinite chain structure taken from Sr_3NiIrO_6 (6) is shown in Fig. 1, where the Ir^{4+} ions with a smaller radius occupy the octahedral site and the Ni^{2+} ions, which are larger, occupy the prismatic site. The 1D character of the BO_6–$B'O_6$ chains is enhanced by the presence of the counter cations, A, which widely separate chains from each other. However, such 1D character is lost and 3D character appears instead when the B cations are nonmagnetic as in Sr_3BIrO_6 ($B =$ Sr, Ca, Zn, Cd, Li, Na) (7) and A_3BRuO_6 ($A =$ Ca, Sr, $B =$ Li, Na) (8), because the intrachain B'–B' interaction is of a comparable magnitude with the interchain B'–B' interactions.

In this paper we report on the synthesis, structure, and magnetic properties of Ca_3NiMnO_6 (CNMO), Ca_3ZnMnO_6 (CZMO), and Ca_3ZnCoO_6 (CZCO) which contain 3d transition metals at both the B and the B' sites. The magnetic properties of the two Mn-containing oxides will be compared in terms of the magnetic dimensionality. The successful synthesis of CZCO is the first exemplification showing the usefulness of a high pressure technique to search for new oxides of this type. To our knowledge it is only $Ca_3Co_2O_6$ (9) that contains 3d transition metals at both B and B' sites. According to the latest works (10–12), the B' site Co ions are nonmagnetic, while the B site Co ions carry a localized moment with a strong anisotropy. The intra- and interchain interactions are ferromagnetic and antiferromagnetic, respectively, and the total magnetism has been characterized in terms of ferromagnetic Ising spin

---

[1]To whom correspondence should be addressed.

[2]Present address: Department of Synchrotron Radiation Research (SPring-8), Japan Atomic Energy Research Institute (JAERI), Mihara, Mikazuki, Sayo-gun, Hyogo 679-5143, Japan.
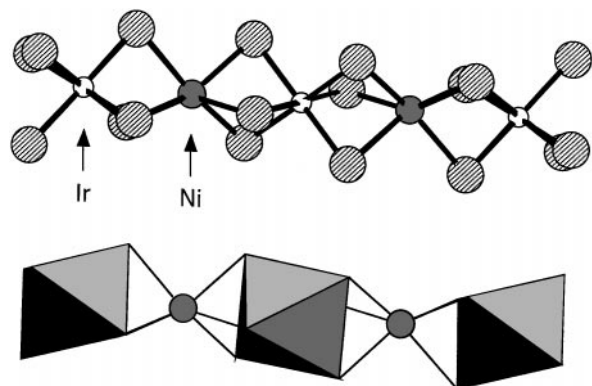
FIG. 1. Alternating chain structure for Sr$_3$NiIrO$_6$ (Ref. (6)) illustrated in two ways. The octahedral coordination of Ir is shown explicitly in the second illustration.

chains and their ferrimagnetic ordering. The present oxides CNMO and CZMO will provide us with Heisenberg spin systems because the single-ion anisotropy is known to be small for both Ni^{2+} and Mn^{4+}.

EXPERIMENTAL

Polycrystalline samples were prepared as follows using a citrate sol-gel precursor technique to improve reactivity and chemical homogeneity. First, CaCO$_3$, metallized Mn (or Co), and Ni (or ZnO), each with a purity of 99.9%, were dissolved in a concentrated nitric acid, to which citric acid and ethyl ether were subsequently added for sol formation. The solution was gradually heated at $100 \sim 350°$C for evaporation and metamorphosis into the gel form. The gel was then decomposed into oxide powder by heating it at $600°$C for 12 h in an oxygen stream of atmospheric pressure.

CNMO and CZMO were obtained from the decomposed gels by adding a process of grinding, pelletization, and heating in the air at $900°$C for 48 h in total. On the other hand, a high pressure process was applied to the preparation of CZCO: The decomposed gel was heated at $900°$C in the air, and the product was then ground, sealed in a gold capsule with an oxidizer, KClO$_4$, and heated at $900°$C for 30 min under 6 GPa by using a cubic anvil-type high pressure apparatus. The oxidizing atmosphere generated by KClO$_4$ was necessary for the oxidation of Co.

X-ray diffraction (XRD) data on powdered samples were collected by using CuKα radiation (Rigaku, RINT 2500) at room temperature. An angular range from 3 to $70°$ in 2θ was scanned in steps of $0.02°$. Magnetization (M) was measured using a SQUID magnetometer (Quantum Design, MPMS XL) at temperatures of $5 \leq T \leq 300$ K in steps of 5 K in an external field of $H = 10$ kOe. Isothermal field dependence at 5 K was measured using another type of SQUID magnetometer (Quantum Design, PPMS) for $-90 \leq H \leq 90$ kOe in steps of 2 kOe.

Neutron diffraction (ND) patterns were collected for CZMO and CNMO at 300 and 10 K from 5 to $165°$ in 2θ with a step interval of $0.05°$ on the high resolution powder diffractometer installed at the research reactor JRR3M, Japan Atomic Energy Research Institute (Tokai). The wavelength used was 2.3005 Å. The samples contained in vanadium cans, 10 mm in diameter and He-filled, were cooled by a conventional ^{4}He closed cycle refrigerator. All the patterns were analyzed using the Rietveld refinement program RIETAN (13, 14), except the magnetic patterns of CNMO measured at 10 K which was analyzed using FullProf (15). In these refinements, the background was fitted with a 6-term polynomial for CNMO and a 9-term polynomial for CZMO, and a pseudo-Voigt peak shape function was employed. The magnetic form factors of Mn^{4+} and Ni^{2+} were used to calculate the magnetic scattering amplitude. The temperature dependence of magnetic Bragg reflections was also measured on the triple axis spectrometer TAS-1 installed at JRR3M. A pyrolytic graphite filter was used in order to reduce higher-order contaminations. The samples were loaded on a cryostat of the same type as used in the HRPD experiment.

RESULTS AND DISCUSSION

The XRD measurement on CNMO, CZMO, and CZCO and also the ND measurement on CNMO and CZMO indicated that all these new oxides crystallize in the Sr$_3$NiIrO$_6$ structure of space group $R\bar{3}c$ (6), though we note here that very small amounts of impurities including NiO and unidentified phases were present depending upon the sample. The Rietveld refinements of the ND data at 300 K, including 52 independent peaks for CNMO and 53 independent peaks for CZMO from which the impurities were excluded, converged well. The isotropic thermal parameters and the occupation factors were refined under a constraint that both 6a and 6b sites were fully occupied.

The observed, calculated, and difference ND patterns are shown in Fig. 2 for CNMO and in Fig. 3 for CZMO. The crystallographic data, selected interatomic distances and bond angles, and other relevant parameters are summarized in Table 1. The lattice constants are considerably smaller than those for the phases containing 4d or 5d metals (2–8) as can be seen in the table. There was no sign of the transition metals being disordered over the two different sites within experimental error (Table 1b): The Ni and Zn ions occupy the prismatic site and the Mn ions occupy the octahedral site. The sharp magnetic transitions found in these oxides by ND (to be shown in Fig. 6) also support the good microscopic homogeneity in these oxides. Concerning CZCO, we have no analytical data but the similarity in ionic radius between Ni^{2+} (0.69 Å) and Zn^{2+} (0.74 Å) and between Mn^{4+} (0.53 Å) and Co^{4+} (0.53 Å) suggests that the ordering in this oxide is as good as in CNMO and CZMO.
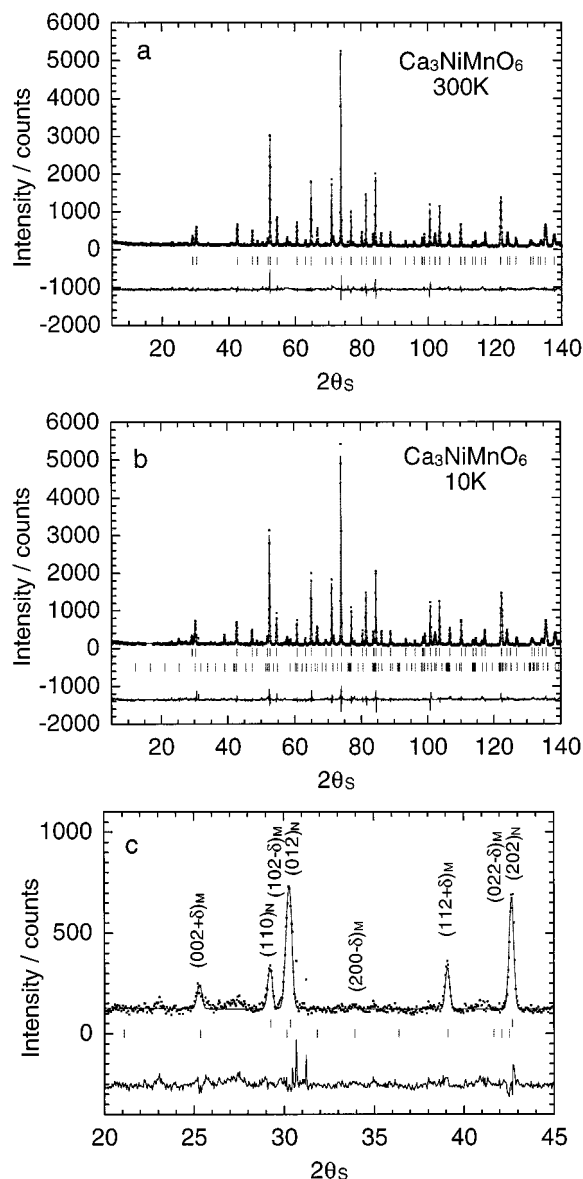
FIG. 2. Observed (dots), calculated (full line), and difference neutron diffraction profiles for Ca_3NiMnO_6 at 300 K (a) and 10 K (b and c). Profile (c) is an enlargement of a certain low scattering-angle part of profile (b). Magnetic reflections are indicated by M, nuclear reflections by N.

ions by the nonmagnetic Zn ions breaks the major exchange path efficiently. Second, the experimental effective magnetic moments, $\mu_{\text{eff}}^{\text{exp}}$, approximate to the expected values, $\mu_{\text{eff}}^{\text{cal}}$, which were calculated assuming $S = 1$, 0, 3/2, and 1/2 for Ni^{2+}, Zn^{2+}, Mn^{4+}, and Co^{4+} in low spin state (t_{2g}^5), respectively. Third, CNMO showed a broad peak around 100 K suggesting short-range ordering due to its 1D AF nature. Below 50 K the magnetization increased but the increase slowed down around 20 K. The anomaly at 20 K corresponds to the long range ordering found in the ND measurement which will be described later. CZMO began to deviate
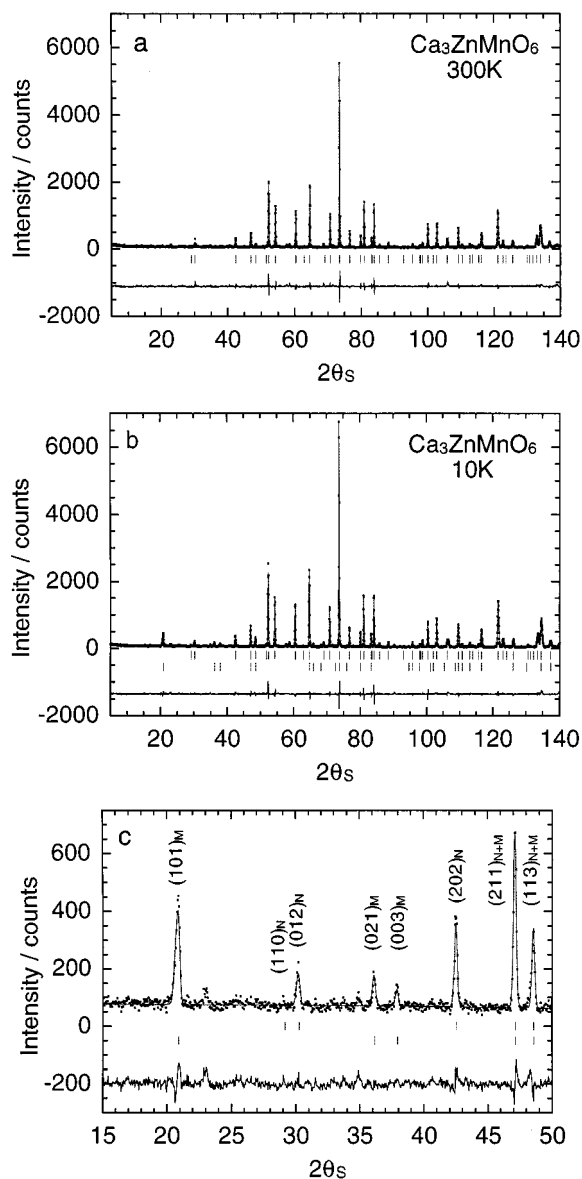

FIG. 3. Observed (dots), calculated (full line), and difference neutron diffraction profiles for Ca_3ZnMnO_6 at 300 K (a) and 10 K (b and c). Profile (c) is an enlargement of a certain low scattering-angle part of profile (b). Magnetic reflections are indicated by M, nuclear reflections by N.

The normal and reciprocal plots of the M–T curves taken at $H = 10$ kOe and the field dependence of magnetization are shown in Fig. 4. The high-temperature M–T data for all these oxides could be fitted to the Curie–Weiss law, and the best fit parameters are listed in Table 2a. These results can be summarized as follows. First, the Weiss temperature, Θ, changes its sign depending upon the oxide indicating that the major interaction is antiferromagnetic (AF) for both CNMO and CZMO and ferromagnetic (FM) in CZCO. The Weiss temperature, Θ, of CNMO is about seven times as large as that of CZMO, revealing that the replacement of Ni

TABLE 1

Crystal and Magnetic Data Determined by Neutron Diffraction at 300 and 10 K for Ca₃NiMnO₆ and Ca₃ZnMnO₆ and the Lattice Parameters for Ca₃ZnMnO₆ Determined by X-Ray Diffraction at 300 K

(a) Lattice parameters

Compounds		a (Å)	c (Å)	R_{wp} (%)	R_p (%)	S (%)	R_F (%)
Ca₃NiIrO₆[a]	(298K)	9.5806(1)	11.1315(2)	—	—	—	—
	(10K)	9.5783(1)	11.1321(2)	—	—	—	—
Ca₃NiMnO₆	(300K)	9.1250(4)	10.5825(3)	11.57	8.71	1.560	3.39
	(10K)	9.0958(2)	10.5671(2)	13.40	9.91	1.8	4.74
Ca₃ZnMnO₆	(300K)	9.1494(5)	10.6323(4)	15.78	11.74	1.636	4.24
	(10K)	9.1282(3)	10.6133(3)	13.84	10.33	1.549	2.84
Ca₃ZnCoO₆	(300K)	9.09(2)	10.61(4)	—	—	—	—

(b) Atomic Positions of Ca at 18e (x, 0, 1/4) and O at 36f (x, y, z), Occupation Factors, g, and Isotropic Thermal Parameters, U_{iso} (Å²), for Ca₃BMnO₆ (B = Ni, Zn)

	Ca₃NiMnO₆			Ca₃ZnMnO₆	
	(300 K)	(10 K)		(300 K)	(10 K)
Ca (x)	0.362(2)	0.3621(4)	Ca (x)	0.363(3)	0.363(1)
O (x)	0.180(2)	0.1800(3)	O(x)	0.179(2)	0.180(1)
O (y)	0.028(2)	0.0273(3)	O (y)	0.025(2)	0.025(1)
O(z)	0.108(1)	0.1084(2)	O (z)	0.107(1)	0.1075(6)
g (Ni, 6a)	1.00(5)	—	g (Zn, 6a)	1.04(9)	—
g (Mn, 6a)	0.00	—	g (Mn, 6a)	−0.04	—
g (Ni, 6b)	0.00	—	g (Zn, 6b)	−0.00	—
g (Mn, 6b)	1.00(4)	—	g (Mn, 6b)	1.00(9)	—
Ca(U_{iso})	1.7(8)	0.9(1)	Ca (U_{iso})	1.1(8)	1.1(4)
Ni (U_{iso})	1.2(6)	0.7(5)	Zn (U_{iso})	0.6(9)	0.6(9)
Mn (U_{iso})	1.4(12)	0.2(6)	Mn (U_{iso})	0.4(12)	0.4(12)
O (U_{iso})	1.1(6)	0.65(7)	O (U_{iso})	0.8(6)	0.7(3)

(c) Selected Interatomic Distances (Å) and Bond Angles (°) at 300 K

	Ca₃NiMnO₆		Ca₃ZnMnO₆
Ni–Mn	2.6456(1)	Zn–Mn	2.6581(1)
Ni–O (×6)	2.14(1)	Zn–O (×6)	2.16(2)
Mn–O (×6)	1.91(1)	Mn–O (×6)	1.92(2)
Ni–O–Mn (×3)	81.3(5)	Zn–O–Mn (×3)	81.1(7)
O–Mn–O (×6)	87.7(6)	O–Mn–O (×6)	88.2(6)
(×6)	92.3(6)	(×6)	91.8(6)

[a] Ref. (6).

from Curie–Weiss behavior below 50 K and then exhibited a small anomaly around 20 K, which also corresponds to the long range ordering taking place at 25.5 K according to the ND measurement.

On the other hand, CZCO showed a FM nonlinearity in the field dependence of magnetization below 90 K (Fig. 4d), but hysteretic field dependence appeared only below 25 K as seen in Figs. 4b and 4d. There seem to be two possible interpretations, one assuming long range FM ordering at 90 K with a small coercivity and the other assuming the development of FM short range ordering at 90 K and sub-

sequent long range ordering setting in at 25 K. The field dependence of magnetization at 5 K (Fig. 4d) is not so simple, showing a change in slope around 30 kOe. There might be a field-induced change in the spin structure. Using the linear part above 70 kOe, a spontaneous moment of 0.6 μ$_B$/Co was estimated. Detailed measurements on single crystals would be interesting.

Both CNMO and CZMO were found to be in a magnetically ordered state at 10 K from the appearance of magnetic Bragg peaks in the ND patterns shown in Figs. 2c and 3c. Those of CNMO shown in Fig. 2c are located near the (002), (102), and (112) positions but could better be indexed by assuming an incommensurate spiral magnetic structure with a single propagation vector (0, 0, 2 + δ) with δ ∼ 0.02. The propagation vector of being close to (002) implied the essential equivalence of the ordered moments located at (x, y, z) and (x, y, z + 1/2) to each other; that is, the Mn moments in a chain were nearly parallel to each other and so were the Ni moments. The absence of any ($hk0 ± δ$) reflections, on the other hand, indicated that the Ni and Mn moments were coupled almost antiparallel to each other, FullProf refinements based on this model using 65 independent magnetic reflections quickly converged to R_{wp} = 13.4%, R_p = 9.91%. The final propagation vector and ordered moments we obtained were δ = 0.0185(7), 1.4(2) μ$_B$/Ni, and 2.2(2) μ$_B$/Mn. The magnetic structure thus determined is illustrated in Fig. 5a. The ordered moments lie in the ab-plane. The in-plane spin direction of the same kind of ion, either Mn or Ni, changes by nearly 120° from chain to chain. In further detail, the Mn moments at (x, y, 0) and (x, y, 1/2) within a chain make an angle of 3.3° to each other, so do the Ni moments at (x, y, 1/4) and (x, y, 3/4), and the moments of the nearest-neighboring Mn and Ni ions are inclined by 181.67° from each other. The incommensurateness must result from a competition of the major intrachain interaction with the minor but nonnegligible interchain interactions.

The magnetic Bragg peaks of CZMO could be indexed in space group $R\bar{3}$. The absence of c-glide reflection indicated that the two Mn ions located at (0, 0, 0) and (1/2, 1/2, 1/2) in the original rhombohedral unit cell were no longer equivalent to each other. Therefore, we started from a two-site collinear AF structure such as that shown in Fig. 5b. The refinement done using 29 independent magnetic reflections showed a good convergence to R_{wp} = 13.84% and R_p = 10.33%, where the ordered moments were assumed to lie in the ab-plane. A Mn moment of 2.43 (15) μ$_B$ was obtained. The spin direction in the ab-plane remained unknown. From the temperature dependence of certain magnetic reflections shown in Fig. 6 one can see that the 3D ordering sets in at 19 and 25.5 K for CNMO and CZMO, respectively.

Here we compare the magnetic dimensionality in the two Mn-containing oxides, CZMO and CNMO. In the chains in
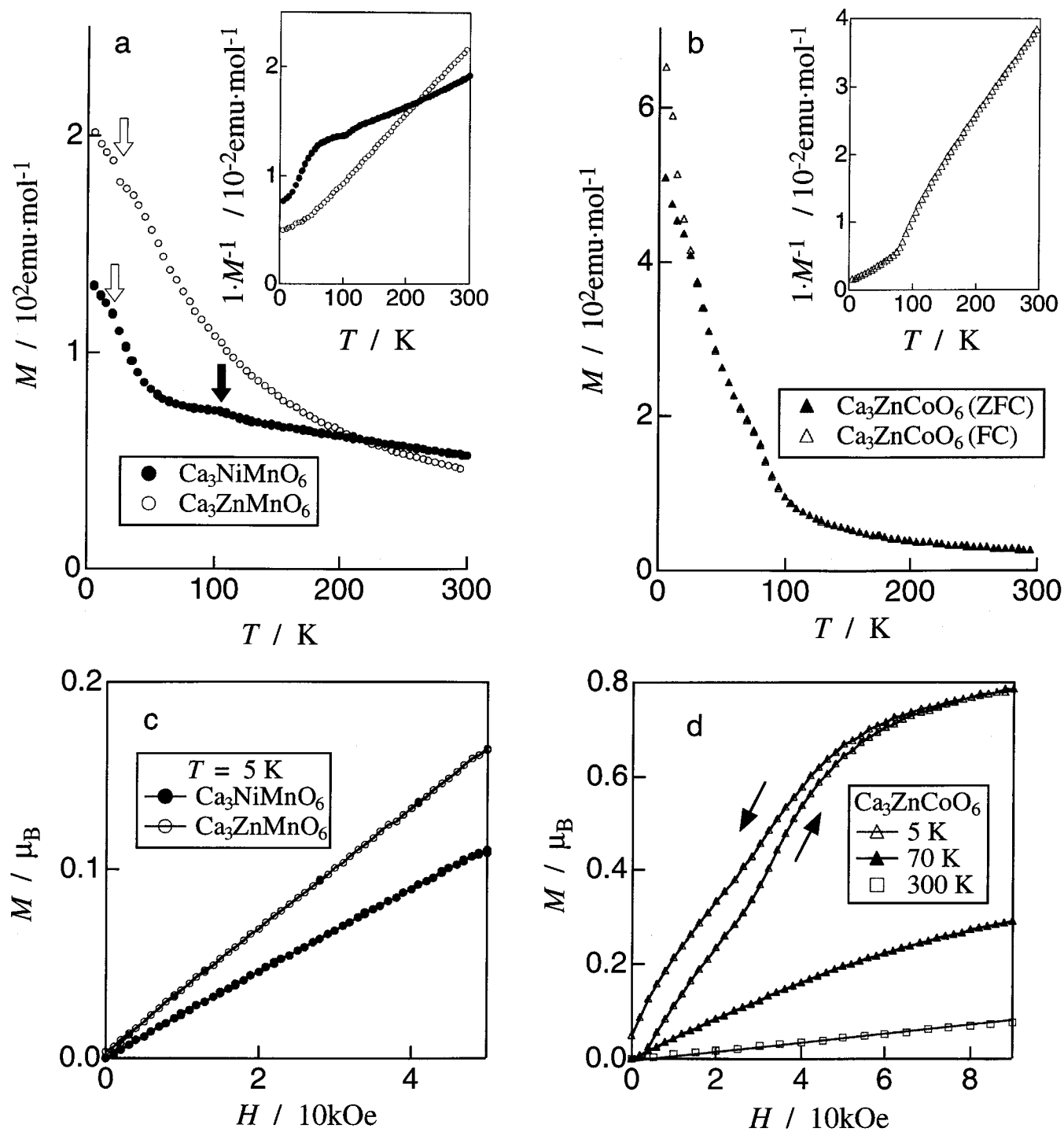
FIG. 4. Temperature dependence of magnetization (M) measured at $H = 10$ kOe and its reciprocal ($1/M$, inset); (a) for Ca_3NiMnO_6 (●, field cooled) and Ca_3ZnMnO_6 (○, field cooled) and (b) for Ca_3ZnCoO_6 (△, zero-field cooled, ▲, field cooled). The dark arrow for Ca_3NiMnO_6 in (a) indicates an anomaly due to short range ordering and the open arrows for Ca_3NiMnO_6 and Ca_3ZnMnO_6 indicate the temperatures of long range ordering determined by neutron diffraction (see Fig. 6). Shown in (c) and (d) are the M–H curves measured at 5 K for Ca_3NiMnO_6 and Ca_3ZnMnO_6 (c) and at 5, 70, and 300 K for Ca_3ZnCoO_6 (d).

TABLE 2
Magnetic Parameters Evaluated from the Curie–Weiss Fitting of Susceptibility and the Ordered Magnetic Moments Determined by Neutron Diffraction

| | (a) Susceptibility data | | |
	Ca$_3$NiMnO$_6$	Ca$_3$ZnMnO$_6$	Ca$_3$ZnCoO$_6$
C (emu.mol^{-1})	3.27(2)	1.56(1)	0.618(1)
Θ (K)	− 326(3)	− 46.5(2)	26.2(2)
$10^4\chi_0$ (emu.mol^{-1})^a	− 3.33(2)	1.42(1)	2.80(1)
$\mu_{\text{eff}}^{\text{exp}}$ (μ_B)	5.11	3.57	2.22
$\mu_{\text{eff}}^{\text{cal}}$ (μ_B)	4.58	3.87	1.73

| | (b) Ordered magnetic moment at 10 K | |
	Ca$_3$NiMnO$_6$	Ca$_3$ZnMnO$_6$
μ_B/Mn	2.2(2)	2.43(15)
μ_B/Ni	1.4(2)	—

^{a}Temperature-independent term.

CNMO the neighboring Ni and Mn ions interact strongly with each other, while the replacement of Ni by Zn should replace the dominant interaction by the intrachain Mn–Mn interaction over a distance of 5.3 Å or the interchain Mn–Mn interactions over a distance of 5.6 Å. Thus, there would be no doubt that magnetic one dimensionality is much more prominent in CNMO than in CZMO. There are certain evidences that support this argument. The susceptibility of CNMO shows a broad maximum around 100 K, far above T_N, which is suggestive of AF ordering of a short

range nature due to low dimensionality. CZMO, on the other hand, simply follows the Curie–Weiss law down to 50 K. If we roughly estimate the dominant exchange interaction J from the Weiss temperature using the simple molecular field equation of $\Theta = 2zJS(S + 1)/3k$, where z is the number of the exchange paths, we obtain $J = - 39.8$ K for CNMO with $z = 2$ and $J = - 2.3$ K for CZMO with $z = 8$ (two intrachain exchange paths plus six interchain paths). Then, a T_N/Θ is only 0.04 for CNMO but as large as 0.5 for CZMO. Long range ordering must be suppressed in CNMO because of one dimensionality.

CONCLUSION

We synthesized Ca$_3$NiMnO$_6$, Ca$_3$ZnMnO$_6$, and Ca$_3$ZnCoO$_6$ which crystallize in the K$_4$CdCl$_6$ type structure. These oxides contain alternating chains made of BO$_6$ (B = Zn, Ni) trigonal prisms and B'O$_6$ (B' = Mn, Co) octahedra. For the preparation of Ca$_3$ZnCoO$_6$ a high pressure technique was applied.

Ca$_3$NiMnO$_6$ and Ca$_3$ZnMnO$_6$ are antiferromagnets with a T_N of 19 and 25.5 K, respectively. The low T_N and other magnetic features of CNMO reflect the magnetic one dimensionality. The replacement of Ni by Zn made the system magnetically three dimensional. CZMO has a simple collinear antiferromagnetic structure with the ordered moment of 2.43(15) μ_B/Mn lying in the ab-plane. CNMO shows a spiral structure whose propagation vector is (0, 0, 2.0185(7)) with the ordered moments of 2.2(2) μ_B/Mn and
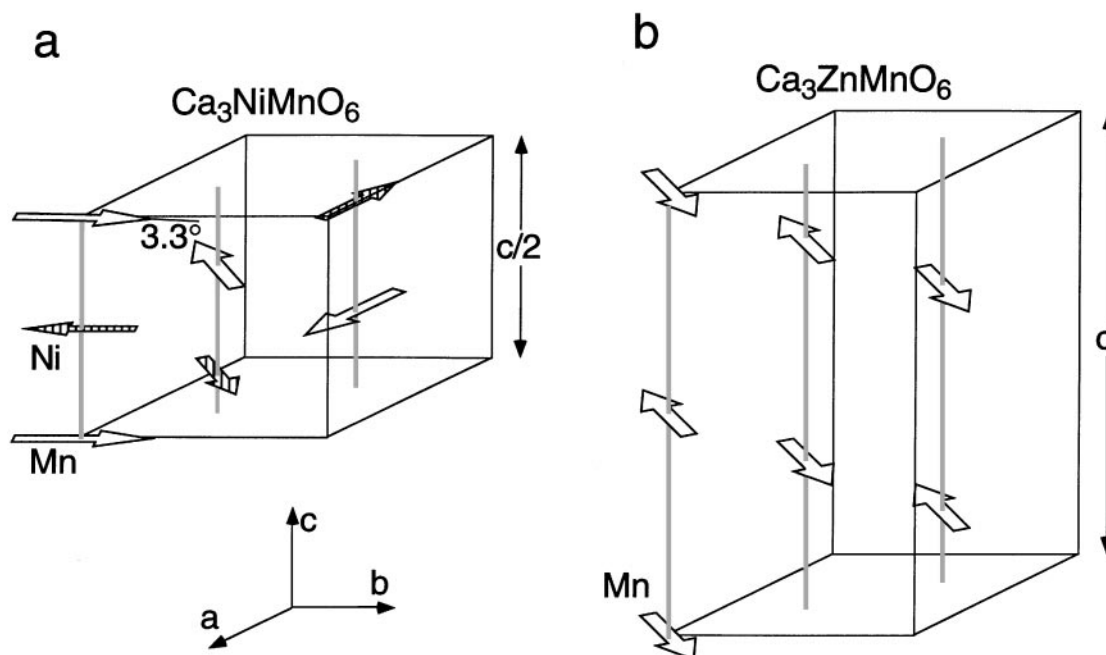

FIG. 5. Spiral magnetic structure for Ca$_3$NiMnO$_6$ (a) and the collinear structure for Ca$_3$ZnMnO$_6$ (b). In both these structures the ordered moments lie within the ab-plane. The spin direction with respect to the a-axis for Ca$_3$ZnMnO$_6$ was not determined.
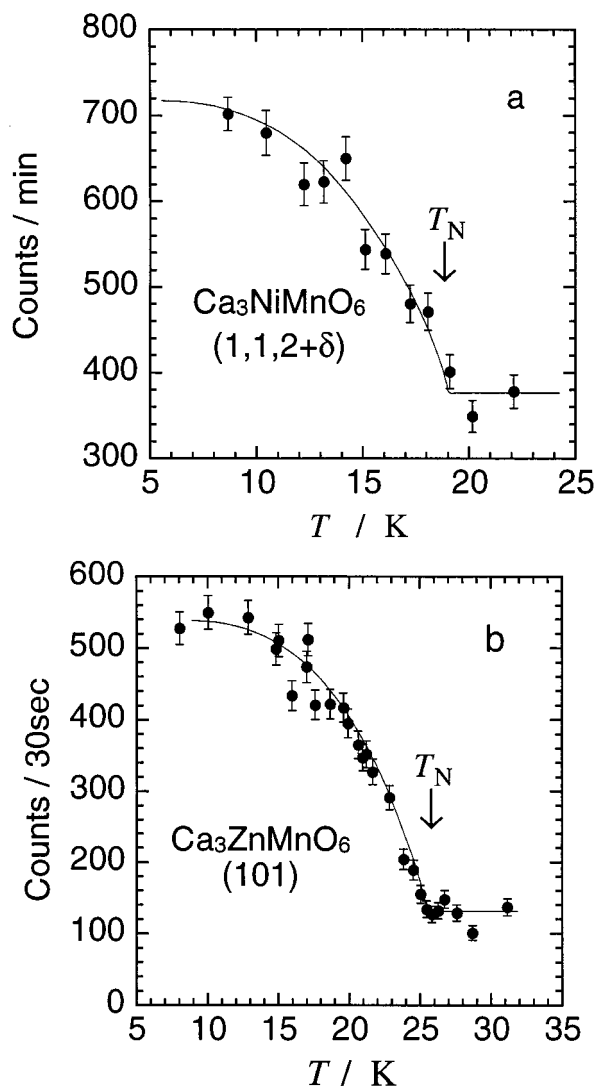
FIG. 6. Temperature dependence of the peak intensity of a magnetic Bragg reflection: $(1, 1, 2 + \delta)$ for Ca_3NiMnO_6 (a) and $(1, 0, 1)$ for Ca_3ZnMnO_6 (b).

1.4(2) μ_B/Ni, both lying in the *ab*-plane. Ca_3ZnCoO_6 began to show FM behavior, though not yet known whether of short ranged nature or long ranged nature, below 90 K. An approximate spontaneous moment of 0.6 μ_B/Co was estimated at 5 K.

REFERENCES

1. G. Bergerhoff and O. Schmitz-Dumont, *Z. Anorg. Allg. Chem.* **284,** 10 (1956).
2. T. N. Nguen, D. M. Giaquinta, and H.-C. zur Loye, *Chem. Matter.* **6,** 1642 (1994).
3. T. N. Nguen and H.-C. zur Loye, *J. Solid State Chem.* **117,** 300 (1995).
4. T. N. Nguen, P. A. Lee, and H.-C. zur Loye, *Science.* **271,** 489 (1996).
5. A. Furusaki, M. Sigrist, P. A. Lee, K. Tanaka, and N. Nagaosa, *Phys. Rev. Lett.* **73,** 2622 (1994).
6. M. Neubacher and Hk. Müller-Buschbaum, *Z. Anorg. Allg. Chem.* **607,** 124 (1992).
7. N. Segal, J. F. Vente, T. S. Bush, and P. D. Battle, *J. Mater. Chem.* **6**(3), 395 (1996).
8. J. Darriet, F. Grasset, and P. D. Battle, *Mater. Res. Bull.* **32,** 139 (1997).
9. H. Fjellvåg, E. Gulbrandsen, S. Aasland, A. Oslen, and B. C. Hauback, *J. Solid State Chem.* **124,** 190 (1996).
10. S. Aasland, H. Fjellvåg, and B. Hauback, *Solid State Commun.* **101,** 187 (1997).
11. H. Kageyama, J. Yoshimura, K. Kosuge, H. Mitamura, and T. Goto, *J. Phys. Soc. Jpn.* **66,** 1607 (1997).
12. H. Kageyama, J. Yoshimura, K. Kosuge, M. Azuma, M. Takano, H. Mitamura, and T. Goto, *J. Phys. Soc. Jpn.* **79,** 3996 (1997).
13. F. Izumi, "The Rietveld Method" (R. A. Young, Ed.), Chap. 13. Oxford University Press, Oxford, 1993.
14. Y.-I. Kim and F. Izumi, *J. Ceram. Soc. Jpn.* **102,** 401 (1994).
15. J. Rodrígues-Carvajal, *Physica B* **192,** 55 (1993).